Elastic properties of porous silicon studied by acoustic transmission spectroscopy

G. N. Aliev,[a] B. Goller, and P. A. Snow
University of Bath, Claverton Down, BA2 7AY, United Kingdom

(Received 4 April 2011; accepted 18 July 2011; published online 31 August 2011)

The porosity dependence of the elastic properties of porous silicon in different crystallographic directions is studied. The velocity of longitudinal acoustic waves in porous silicon layers electrochemically etched in (100), (110), and (111) oriented wafers has been measured by acoustic spectroscopy in the gigahertz frequency range. This non-destructive method was used for porous silicon layers with porosity of 25−85% obtaining velocities in the range of about 1 to 7 km s^{-1}. The implication of constant Poisson's ratio of porous silicon is examined. The effect of velocity dispersion due to multiple scattering is considered. The c_{11} stiffness constant can be obtained from the velocity measurement in the [100] direction of a cubic crystal. We show that, using the results for velocity in [110] or [111] directions and Keating's relation, the stiffness constants c_{12} and c_{44} can be obtained. The velocity dependence on porosity was fitted as $v = v_0(1-\phi)^{\kappa}$, where v_0 is the velocity in bulk silicon, ϕ is porosity, and κ is a fitting parameter. It is shown that with other conditions being equal: (i) the porosity dependence of the acoustic velocity is related to the doping level of the wafer from which the porous silicon was etched (κ depends on wafer resistivity); (ii) acoustic velocities in different crystallographic directions have the same dependence on porosity (κ is independent of wafer orientation). This requires that all three stiffness constants c_{11}, c_{12} and c_{44} have the same dependence on porosity: $c_{ij} = c_{ij}^0(1-\phi)^m$; and (iii) the morphology of porous layers depends on the HF concentration in the etchant (κ is used as an indicator for the disorder of the porous structure). © *2011 American Institute of Physics*. [doi:10.1063/1.3626790]

I. INTRODUCTION

In recent years there has been much interest in porous materials. These materials range from naturally occurring solids such as rock, wood, and bone to artificial materials such as concrete, sintered ceramics, aerogels, and metal foams that require optimization of their properties to help in their technical applications. Many examples are available over only a limited range of porosity (the volume fraction of voids) and a percolation threshold may exist, indicating a critical porosity, after which the material mechanically fails. A sub-class of porous materials are cellular solids for which the properties of the whole material is understood in terms of the properties of the material of the walls or struts of the cells modified by the topology of the cells. The key parameter is the relative density of the cellular solid compared to the wall material; i.e., the porosity of the solid. This class of materials is reviewed in the classic work by Gibson and Ashby[1] examining their mechanical, electrical and thermal properties.

Porous silicon (PSi) is a material whose morphology can be controlled during the process of manufacture. It can be prepared by electrochemical etching of high-quality crystalline Si wafers. The current-driven etching breaks Si-Si bonds as pores penetrate into the volume of the wafer. Thus, open pores are produced surrounded by a relatively unperturbed Si structure. The properties of the walls are those of anisotropic bulk Si. The pores are tunable from micropores (<2 nm) and mesopores (2−50 nm) to macropores (>50 nm). The porosity can be varied from 4% for macroporous to 95% for mesoporous Si. This range of porosities available for study is an unusual feature for a porous material.

The wafer doping, wafer orientation, HF concentration in etchant, and etching current density all control the morphology of PSi (the structural regularity on macroscopic scale) and the pore size. The doping level, giving a wafer resistivity R, of p-type wafers is usually represented as p^- ($R > 1\ \Omega$ cm) for lightly doped, as p^+ ($R \sim 0.02-1\ \Omega$ cm) for moderately doped, and as p^{++} ($R < 0.02\ \Omega$ cm) for heavily doped samples. PSi can be produced from wafers oriented in any crystallographic direction, but typically commercial wafers are available in the principal cubic orientations of (100), (110), and (111).

It has been proposed that mesoporous (100) PSi has a structure close to that of an open-cell foam[2] with major trunk pore connected by smaller side branches rather than being a honeycomb structure, which is often assumed given the directionality of the (100) pores. For (110) and (111) etched samples, the major trunk pores etch away from the wafer surface in the [100] directions. This gives a different morphology for samples etched on different orientations but one which reflects the symmetry of Si and is equivalently cellular. The observed length of pores compared to the cross-branching ratio suggests formation of elongated pores in the Si foam.

It has been found that the crystal symmetry of PSi is the same as that of Si: cubic, diamond-like, and hence anisotropic. Cullis and Canham[3] measured transmission electron

[a]Author to whom correspondence should be addressed. Electronic mail: g.aliev@bath.ac.uk.

diffraction patterns from four (001) oriented highly porous (~80%) samples. They note that the sample etched from a p^{++} wafer (0.005 Ω cm) shows a diffraction pattern very similar to that of perfect bulk Si. For the sample etched from a p^{-} wafer (40 Ω cm) the diffuse diffraction spots showed strong arcing and streaking. This was interpreted as a component of disoriented material in the sample, possibly due to static distortions of Si wires, with some broadening due to small crystallite sizes in the PSi. In a detailed investigation of samples with porosity 34%–78% Metzger *et al.*[4] used small angle X-ray scattering and, on lower porosity samples, grazing incidence diffraction of synchrotron radiation. They found PSi layers etched from a p^{++} wafer (0.010 Ω cm) to be predominantly large cylindrical particles forming a perfect lattice around the pores, while a PSi layer etched from a p^{-} wafer (10 Ω cm) was interpreted as a network of coherently connected particles that form a pseudomorphically strained Si lattice around the pores.

The tunability of porosity means that physical properties of the porous layers are also tunable. The control of refractive index with porosity has been exploited for many years in various classes of optical devices.[5] However, after two decades of intensive study of PSi, the porosity dependence of its elastic and acoustic properties are still not well understood.

The elastic and acoustic properties of PSi, namely the stiffness constants, Young's modulus and acoustic velocity (shear and longitudinal) have been examined as a function of porosity in several earlier works by different methods: acoustic microscopy,[6,7] microechography,[8,9] Brillouin scattering,[10–14] X-ray diffraction,[15] nanoindentation,[2] and laser ultrasonic interferometry.[16] Conflicting results for sound velocities in PSi can be found in this literature.

It has been suggested that the sound velocity in PSi layers, electrochemically etched on wafers of different resistivity, varies due to differences in the morphology of the layers.[2,9,13] However, no conclusive research has been performed on this proposal.

A thorough understanding of the mechanical properties of PSi is needed for new applications. Work has started on using PSi for MEMS applications, for example, a pressure and temperature sensor based on the deformation of a PSi diaphragm.[17] Recent work has demonstrated acoustic Bragg mirrors and rugate filters that indicate that PSi layers could be employed in bulk acoustic wave devices, such as the solidly mounted resonators used in wireless communications systems.[18,19]

In this work, the elastic properties of mesoporous PSi have been studied by measurement of the porosity dependence of the longitudinal acoustic (LA) velocity for several sets of PSi samples electrochemically etched on boron-doped Si wafers of different doping level and crystallographic orientations. We also present an example for the dependence of elastic properties of PSi on the HF concentration in the etchant, which gives an additional degree of freedom to tailor the properties of PSi.

II. THEORY

To understand the porosity dependence of the elastic properties of PSi, we will first discuss general features observed in theories for the elasticity of cellular materials. These theories are typically semiempirical. For PSi, which retains its Si lattice structure in the solid skeleton around the pores, we show how the porosity dependence of the elasticity can be incorporated into the representation of an anisotropic cubic material. We then propose some features of the elasticity of PSi that are consistent with our results. Additionally, we estimate the effect of multiple scattering on results obtained from acoustic measurements.

A. Young's modulus and Poisson's ratio of cellular solids

For cellular solids, Gibson and Ashby[1] propose a semiempirical relation between Young's modulus E and density ρ:

$$E/E_0 = C(\rho/\rho_0)^m, \tag{1}$$

where E_0 and ρ_0 are the Young's modulus and density of the bulk material. The index notation "0" will be used for the rest of this paper to indicate the value for bulk Si. Relative density can be expressed as $\rho/\rho_0 = 1 - \phi$, where ϕ is porosity.

Equation (1) describes Young's modulus for many types of foams. The constants C and m depend on the microstructure of the solid. Typically, for cellular solids m ranges between 1 and 4 giving a wide range of possible elastic properties for a given porosity (see discussion by Roberts and Garboczi[20]). For open-cell foams, experimental results supported by a model of bending beams[1] suggest that $C = 1$ and $m = 2$, while for honeycomb structures $m = 1$.

For Poisson's ratio, ν, Gibson and Ashby[1] assume $\nu \sim 1/3$ independent of porosity for open cells. Roberts and Garboczi[20] for three-dimensional open-cell solids and Dunn and Ledbetter[21] for randomly oriented closed spherical and needle-shape pores have shown that ν will be nearly independent of porosity when ν_0 is close to 0.2. Herakovich and Baxter[22] have shown that, for open-cell material with elongated pores with a square cross section, ν is independent of porosity.

Overall, we conclude that for porous open-cell structures for which the skeleton material has $\nu_0 \sim 0.2$, there is a weak or no dependence of ν on porosity. In analysis of X-ray data for PSi, Barla *et al.*[15] assumed a constant ν for a porosity range of 34% to 72%, however at the value of 0.1 that is inconsistent with the works cited above. ν for bulk Si is given below (Sec. II B) for different crystallographic directions and can be seen to average to ~0.22. Thus, we will assume that ν in any crystallographic direction is independent of porosity and identical to that of bulk Si in a certain direction.

B. Young's modulus and Poisson's ratio of cubic crystals

In any direction through a cubic crystal, Young's modulus is given in terms of three compliances s_{ij} and directional cosines.[23] For the three crystallographic directions measured in our experiments:

$$1/E_{[100]} = s_{11},$$
$$1/E_{[110]} = s_{11} - \tfrac{1}{2}S, \quad (2)$$
$$1/E_{[111]} = s_{11} - \tfrac{2}{3}S,$$

where $S = s_{11} - s_{12} - \frac{1}{2}s_{44}$. For isotropic solids $S = 0$ and $E = 1/s_{11}$. Compliances s_{ij}^0 and stiffnesses c_{ij}^0 for bulk Si are given in Table I (from Ref. 24).

Poisson's ratio for extensions along the principal directions mentioned above is given as[25]

$$\nu_{[100]} = -s_{12}/s_{11},$$
$$\nu_{[110]}^{21} = -(s_{12} + \tfrac{1}{2}S)/(s_{11} - \tfrac{1}{2}S),$$
$$\nu_{[110]}^{31} = -s_{12}/(s_{11} - \tfrac{1}{2}S), \quad (3)$$
$$\nu_{[111]} = -(s_{12} + \tfrac{1}{3}S)/(s_{11} - \tfrac{2}{3}S),$$

where upper indices denote the two axes (x_k) orthogonal to the direction of extension. The values for bulk Si are $\nu_{0[100]} = 0.28$, $\nu_{0[110]}^{21} = 0.064$, $\nu_{0[110]}^{31} = 0.36$, and $\nu_{0[111]} = 0.18$ (with an average value of 0.21 for [110]-direction). For polycrystalline silicon, which is isotropic, the typical value measured is $\nu_{poly} = 0.22$ (Ref. 24), which is the average value overall directions for crystalline Si.

Using relations between s_{ij} and c_{ij} given in Ref. 23 Young's modulus and corresponding Poisson's ratio for [100]-direction can be written in terms of stiffnesses as

$$E_{[100]} = (c_{11} - c_{12})(c_{11} + 2c_{12})/(c_{11} + c_{12}), \quad (4)$$

$$\nu_{[100]} = c_{12}/(c_{11} + c_{12}). \quad (5)$$

From Eqs. (4) and (5) one can obtain

$$E_{[100]} = c_{11}(1 + \nu_{[100]})(1 - 2\nu_{[100]})/(1 - \nu_{[100]}). \quad (6)$$

Equations (4)–(6) are similar to those which are commonly presented and used for isotropic solids having a single value of ν and E.

C. Sound velocity in cubic crystals

Acoustic velocities in solid crystals are obtained using c_{ij} and angle of propagation to the principal axes.[26] The expressions for wave velocity along the three principal axes of cubic crystal are shown in Table II.

Assuming $\nu_{[100]}$ is independent of porosity, one can obtain from Eq. (6):

$$E_{[100]}/E_{0[100]} = c_{11}/c_{11}^0. \quad (7)$$

For the LA velocity in [100] direction, using Eq. (1) with C = 1, Eq. (7) and Table II we obtain the well-known semi-empirical formula:

TABLE I. Elastic constants of bulk silicon at room temperature.

c : GPa s : 10^{-12}Pa^{-1}	c_{11}	c_{12}	c_{44}	s_{11}	s_{12}	s_{44}	S
bulk Si	165.6	63.9	79.5	7.68	−2.14	12.6	3.52

TABLE II. Sound velocities in different directions of wave propagation in cubic crystals. Lower indexes: L: longitudinal, T: transverse. For waves in [110] direction: $T_\parallel$: polarized in [001] direction, $T_\perp$: polarized in $[1\bar{1}0]$ direction.

	[100]	[110]	[111]
v_L^2	$\frac{c_{11}}{\rho}$	$\frac{c_{11}+c_{12}+2c_{44}}{2\rho}$	$\frac{c_{11}+2c_{12}+4c_{44}}{3\rho}$
$v_{T_\parallel}^2$	$\frac{c_{44}}{\rho}$	$\frac{c_{44}}{\rho}$	$\frac{c_{11}-c_{12}+c_{44}}{3\rho}$
$v_{T_\perp}^2$	$\frac{c_{44}}{\rho}$	$\frac{c_{11}-c_{12}}{2\rho}$	$\frac{c_{11}-c_{12}+c_{44}}{3\rho}$

$$v_L = v_{0L}(1 - \phi)^\kappa, \quad (8)$$

where $\kappa = \frac{1}{2}(m - 1)$. This form of velocity dependence on porosity will be used to fit our experimental results. It is shown below that this formula, with only one fitting parameter κ, fits the experimental data reasonably well, therefore we do not use more complicated models.

We will show that, measuring only LA velocities in any two of the principal directions, all three stiffness constants for a cubic diamond-like crystal can be obtained.

The LA velocities in directions [100], [110], and [111] are not independent. It can be shown, using expressions from Table II, that $v_2^2 = (v_1^2 + 3v_3^2)/4$, where the principal LA velocities are labeled as $v_1 = v_{L[100]}$, $v_2 = v_{L[110]}$, and $v_3 = v_{L[111]}$. Thus, knowing only LA velocities, all three stiffness constants c_{11}, c_{12}, and c_{44} of PSi cannot be obtained independently. However, the stiffness constants themselves are not independent; for anisotropic cubic diamond-like crystals Keating[27] derived the relation: $c_{44} = \frac{1}{2}(c_{11} - c_{12})(c_{11} + 3c_{12})/(c_{11} + c_{12})$. This should be contrasted with the expression for the isotropic case: $c_{44} = \frac{1}{2}(c_{11} - c_{12})$, assumed by some authors[8,12] for PSi. Given the evidence that PSi retains the Si crystal symmetry, we conclude that Keating's relation will at least be a better approximation to the properties of PSi.

Using Keating's relation and expressions from Table II the following relations between stiffness constants and velocity are obtained:

$$c_{11} = \rho v_1^2,$$
$$c_{12} = \rho\left[v_1^2 - \tfrac{1}{2}v_2^2 - \sqrt{\tfrac{1}{4}v_2^4 - 2v_1^2(v_2^2 - v_1^2)}\right], \quad (9)$$
$$c_{44} = \rho\left[\tfrac{3}{2}(v_2^2 - v_1^2) - \sqrt{\tfrac{1}{4}v_2^4 - 2v_1^2(v_2^2 - v_1^2)}\right].$$

Thus, for anisotropic cubic diamond-like crystal, measuring LA velocities in any two directions of [100], [110], and [111] all three stiffness constants can be determined. For isotropic solids, $v_1 \equiv v_2 \equiv v_3 = \sqrt{c_{11}/\rho}$, and it is not possible to obtain all three c_{ij} from only LA velocity measurement.

D. Velocity dispersion in porous material due to multiple scattering

As discussed by Truell *et al.*,[28] the phase velocity in a medium with scatterers analyzed in a multiple scattering (MS) theory is different to that through the same effective medium with no scattering considered.

In the limit of pore size smaller than the wavelength of ultrasound used, Sayers[29] derived an analytic expression for the ultrasonic dispersion in an isotropic porous medium. For mesoporous PSi studied in our work at 1 GHz (see Sec. III), this limit is well fulfilled: $ka < 0.03$, where $k = \omega/v_L$ is the wave number and a is the pore radius. For $ka \ll 1$, the relation between LA velocities v'_L with and v_L without MS considered is given as[29]:

$$v'_L/v_L \approx (1 - \varphi A)^{-1/2}, \tag{10}$$

where $\varphi = \frac{4}{3}\pi a^3 n_0$, n_0 is the concentration of scatterers, $A = 2 - \frac{3}{4}\xi^2 + 5\left(1 - \frac{9}{4}\xi^2\right)^{-1}$ and $\xi = v_L/v_T$.

In spite of the fact that the theory was developed for an isotropic medium, we will apply it to our case of anisotropic PSi neglecting the second order effect of anisotropy. In other words, we assume that ξ is independent of the crystal orientation and $\xi^2 = c_{11}/c_{44}$. As c_{11} and c_{44}, as shown below (Eq. (15) in Sec. IV A), have the same dependence on ϕ for PSi, ξ is independent of ϕ. Thus, using values for bulk Si from Table I we obtain for whole range of porosity: $\xi = 1.44$ and $A = -0.916$.

Although Eq. (10) is derived for spherical voids, it is also correct for voids of any shape (see Ref. 30). For scatterers of different shape, e.g., an ellipsoid, a cylinder, and a right prism, with the aspect ratio ζ, φ can be expressed in terms of porosity as ϕ/ζ, $\frac{2}{3}\phi/\zeta$, and $\frac{\pi}{6}\phi/\zeta$, respectively ($\varphi = \phi$ for sphere).

Inset (a) in Fig. 1 demonstrates velocity dispersion versus porosity calculated using Eq. (10) for pores with a shape of a right prism with different aspect ratios of 1, 2, and 3.

Thus, if we are to consider velocity dispersion due to the effect of MS then in order to calculate elastic constants using Eqs. (9) we have to obtain v_L from measured velocities v'_L using Eq. (10).

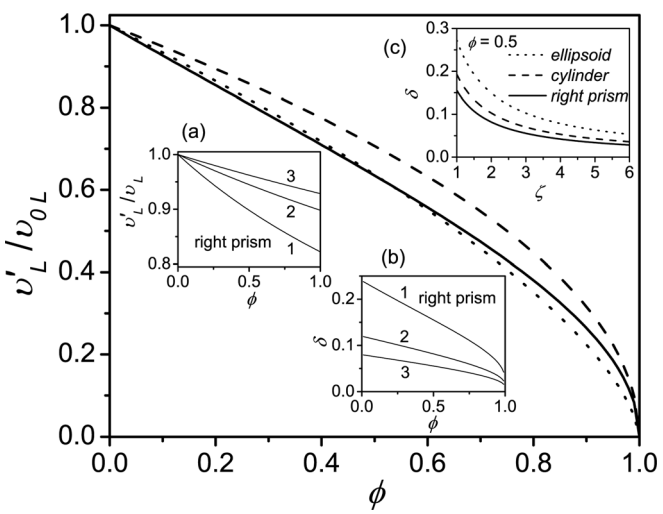

FIG. 1. Porosity dependent effect of multiple scattering for pores of the cubic shape ($\zeta = 1$). Solid line from Eq. (11) with $\kappa' = 0.5$, dashed and dotted lines from Eq. (12) with $\kappa = 0.5$ and $\kappa = 0.65$, respectively. Insets: (a) v'_L/v_L vs porosity; (b) δ vs porosity. Lines in (a) and (b) are calculated for right prism with the indicated aspect ratios 1, 2, and 3. (c) δ calculated for $\phi = 0.5$ vs aspect ratio of pores with different shape: right prism (solid), cylinder (dashed), and prolate ellipsoid (dotted).

To fit to experimental velocity data two simple techniques are consistent with the previous discussions.

The first way would be to use a formula:

$$v'_L = v_{0L}(1 - \phi)^{\kappa'}(1 - \varphi A)^{-1/2}, \tag{11}$$

with a new fitting parameter κ' and an estimation of probable shape of pores via the form of φ. Figure 1 shows an example of this function for values of $\kappa' = 0.5$ and cubic pores, $\zeta = 1$, which gives an almost linear dependence of v'_L on porosity up to $\phi = 0.7$ as shown by the solid line. We illustrate the effect for $\kappa' = 0.5$ as we consider this as a "lower bound" value for an "ideal" open-cell foam (see Sec. II A). Bellet *et al.*[2] obtained $\kappa' = 0.5$ for Young's modulus of mesoporous PSi by nanoindentation, i.e., "static", experiments.

The second way is to use Eq. (8) with a single fitting parameter κ, with no assumption about the shape of pores, but with an understanding that the κ is slightly different due to the effect of MS. Hence, for fitting to our experimental results, we will use

$$v'_L = v_{0L}(1 - \phi)^{\kappa}. \tag{12}$$

The dotted line in Fig. 1 shows that a close match is obtained to the curve above from Eq. (11) for a value of κ of 0.65.

For the porosity dependence of Young's modulus from Eq. (1) and elastic constants from Eqs. (15), $m = 2\kappa' + 1$ will be used with κ obtained by a correction of κ by the decrement δ:

$$\kappa' \approx \kappa - \delta. \tag{13}$$

We note that from Eqs. (11)–(13) one can obtain: $\delta = -\frac{1}{2}\ln(1 - \varphi A)/\ln(1 - \phi)$. In Fig. 1(b) δ is plotted versus ϕ calculated for pores with the shape of a right prism. We take a value of δ at $\phi = 0.5$ as a mean value for the whole porosity range. For voids with shapes of right prisms with an aspect ratio, say, 1 and 4, the mean values of δ are 0.15 and 0.04, respectively (see inset (c) in Fig. 1). This indicates the order of magnitude of the MS effect for micro- and mesoporous PSi for acoustic measurements up to 20 GHz range.

III. EXPERIMENTAL TECHNIQUE AND RESULTS

In order to systematically investigate the dependence of the LA velocities on the crystallographic direction and the sample morphology, determined by the substrate resistivity, several sets of commercial Si wafers with different resistivity specifications were used. Room-temperature anodization was performed using a 1:1 solution of 49% aqueous-HF and hydrous ethanol, unless indicated otherwise. The thickness d of the layers was controlled by the etch duration time. The layers were etched to thicknesses in the range of $10 - 70\mu$m to give a resolvable ($\geq$5 ns) time-of-flight for sound waves in the porous layer. The thickness of the layers was determined by scanning electron microscopy. The porosity was set by the etching current density and was varied in the range of $0.25 - 0.85$. After etching, the porosity of layers was verified by analysis of Fabry-Pérot interference fringes to obtain the effective optical path length nd of the layer, where n is

the effective refractive index. The effective medium approximation method in Bruggeman formulation[31] was used. Additionally, the porosity and thickness were self-consistently determined by a pore filling technique; two different substances (air and ethanol) were used to fill the pores, thus changing n while the layer thickness and Si content (porosity) were constant.[9]

The LA velocity was obtained by acoustic transmission spectroscopy at room temperature using a vector network analyzer (VNA) with ~ 0.5 ns resolution in the time domain. A specimen was placed between two transducers Tr1 and Tr2 (Fig. 2(a)) operating with a central frequency at 1 GHz. Each transducer consists of a ZnO piezoelectric layer driving waves into a square silicon pillar ($160\,\mu\text{m} \times 160\,\mu\text{m} \times 500\,\mu\text{m}$). Transducers were coupled to the specimen via water or In-Ga eutectic. Penetration of the coupling liquid into pores was not detected and switching from one liquid to the other did not affect the measured sound velocity. Acoustic waves were emitted normally into the PSi layers with uncertainty in alignment of less than 0.5°. Under these conditions, no shear waves were excited in the PSi.

The transducers were connected to two ports of the VNA and transmission parameters were measured as a function of frequency. The equivalent response in the time domain (Fig. 2(b)) was calculated using a fast Fourier transform algorithm. The first peak observed, t_0, is equivalent to a pulse passing directly through the transducers, PSi and Si layer. The later peaks correspond to longer times-of-flight due to reverberation in layers of the structure. In Fig. 2(b) a part of the time response that gives measurable peaks up to ~800 ns after t_0 is shown. We consider PSi as an effective medium for optical and acoustical waves as the wavelength is much greater than the pore sizes of the samples.

The LA phase velocity for the PSi layer can be calculated as: $v'_L = 2jd/(t_j/t_0)$, where d is the thickness of the PSi layer, t_0 and t_j $(j = 1, 2, 3)$ are the arrival times with no and j roundtrips within the PSi layer, respectively (Fig. 2). The obtained velocities are shown in Figs. 3(a)–3(c). Each point is the average of values obtained from all t_j measured on several different places of the specimen. Simultaneously, the

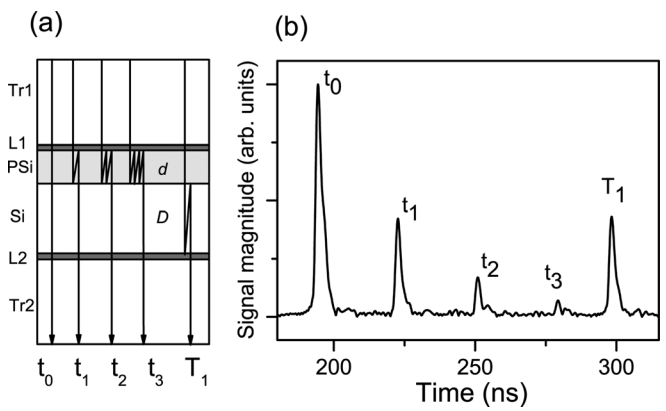

FIG. 2. (a) Schematic illustration of reflection-dependent paths for sound waves in the structure consisting of transducers Tr1 and Tr2, coupling liquids L1 and L2, and PSi layer of thickness d on Si substrate of thickness D; t_0, t_j, $(j = 1, 2, 3)$ and T_1 label times as in (b). (b) Example of transmitted signal amplitude in time domain for the specimen with the parameters: $d = 56.7\ \mu\text{m}$, $D = 474\ \mu\text{m}$, $\phi = 0.7$, $R = 10 - 20\ \text{m}\Omega$ cm, (110)-oriented.

LA velocity for the bulk silicon substrate can be calculated as $v_{0L} = 2D/(T_1 - t_0)$, where D is thickness of the underlaying bulk Si, and T_1 is the arrival time after a single round trip within the substrate (Fig. 2). For Si substrates of (100), (110), and (111) crystallographic orientation, we obtained LA velocities v_{0L} of 8.43, 9.13, and 9.35 km/s, respectively. These results agree with the literature values[32] and are shown in Figs. 3(a)–3(c) at zero porosity.

Our experimental technique allowed us to measure only LA velocity. Our etching method does not produce porous Si layers on which velocities in different crystallographic directions, within the same sample, could be measured (with our technique). Instead, porous layers were etched in standard commercial wafers cut in different directions. During etching, the main pores etch along the (100) direction and the side pores along the (111) direction[33] so the set of pores produced for the (110) and (111) samples are at angles to the surface of the wafer and not fully identical to what would be viewed in the (100) sample in that direction. This variation in micro-morphology does not change the overall symmetry or regularity of the porous structure as shown below.

Figures 3(a)–3(c) show the porosity dependence of LA velocity for the three principal crystallographic directions for a range of doping levels of the starting Si wafer, as indicated in the figure. All results in Figs. 3(a)–3(c) were obtained with the same HF concentration in the etchant. The lines in the figures are obtained by a fit using Eq. (12) to obtain the single fitting parameter κ. The general trend observed is that κ increases as the doping level of the Si wafer decreases.

In Fig. 3(d) the fitting parameter κ is plotted on a semilogarithmic scale versus the resistivity of the Si wafers for all values of κ obtained from all the wafers used, and two points from the literature.[12,14] It can be seen that with other conditions (HF solution, etching temperature, etc) being the same κ does not depend on crystallographic direction but only on wafer resistivity. The dependence shown is logarithmic versus resistivity of the substrate. The error bars in resistivity arise from wafer specification. A line of best fit is shown in Fig. 3(d), given by

$$\kappa = 0.23 \log(R) + 1.15. \tag{14}$$

To demonstrate another degree of freedom for controlling the samples morphology, using (100)-wafers with resistivity of 15–25 mΩ cm, we etched a set of samples varying the volume fraction of aqueous-HF to ethanol (V_{HF}/V_{Eth}). Assuming the validity of Eq. (12), we obtained κ from a velocity measurement on each sample in this set of samples as $\kappa = \ln(v'/v_0)/\ln(1-\phi)$. Results are shown in Inset of Fig. 3(d). The value of κ for $V_{HF}/V_{Eth} = 1$ is obtained by averaging data from Fig. 3(a). To verify nonmonotonic behavior near $V_{HF}/V_{Eth} = 0.75$, we etched several samples with this concentration but of different porosity and thickness. The averaged values are shown with the uncertainty on the value of κ. As can be seen from κ -values, p^{++} samples etched using $V_{HF}/V_{Eth} < 0.5$ exhibit a κ -value, and hence morphology, like typical p^- samples etched using $V_{HF}/V_{Eth} = 1$.

These two results on the effect of wafer resistivity and etchant concentration on the velocity of sound, for any given

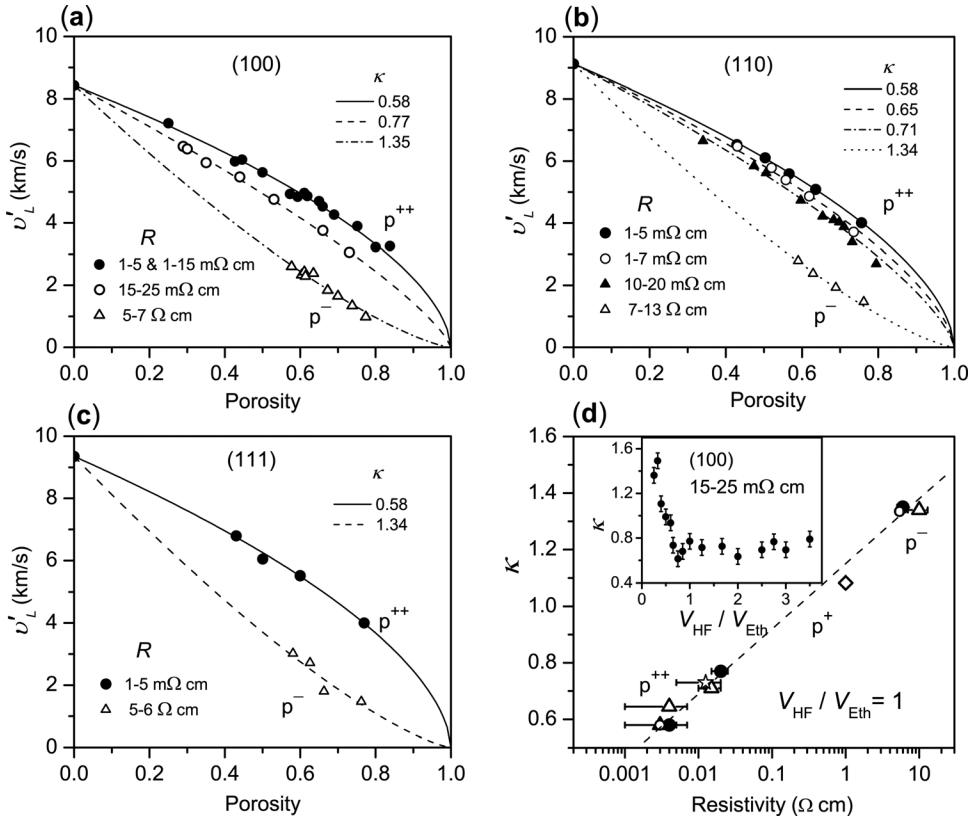

FIG. 3. (a)–(c) Experimental values of LA velocity v'_L in PSi for the layers produced from Si wafers of indicated crystallographic orientation and resistivity are depicted by symbols fitted by $v'_L = v_{0L}(1-\phi)^{\kappa}$ with different fitting parameter κ. (d) Dependence of κ on wafer resistivity. Symbols correspond to samples with orientation: • (100), Δ (110), ○ (111), and from literature ⋆ (100) (Ref. 14) and ◊ (100) (Ref. 12). Inset: κ vs V_{HF}/V_{Eth}, volume ratio of etchant HF to ethanol.

porosity, show that PSi samples must be well specified for the velocity to be predicted. Equally, to achieve a required acoustic velocity for a PSi layer, various parameters can be adjusted. This can also help to explain the diverse velocity results previously reported.

IV. DISCUSSIONS

A. Dependence of elastic constants on porosity

Figure 3 demonstrates that v_i $(i = 1, 2, 3)$ measured for PSi samples etched from wafers with the same resistivity (i.e., having the same level of pore regularity) have the same dependence on porosity ϕ, i.e., the same κ. This can be observed in Figs. 3(a)–3(c) where the same fitting parameter holds for the p^{++} and p^{-} samples in the three crystallographic directions, but is better illustrated in Fig. 3(d) which shows that the general trend is obeyed for all crystallographic directions at different resistivity values.

From Eqs. (9) it is clear that if v_1 and v_2 have the same dependence on ϕ then all three stiffness constants c_{ij} in a cubic crystal must have the same dependence on ϕ and, using Eq. (8), can be expressed as

$$c_{ij} = c^0_{ij}(1-\phi)^m, \tag{15}$$

where $m = 2\kappa' + 1$ has the same meaning as in Eq. (1).

If all the stiffness constants have this form of dependence on porosity then the compliances s_{ij} all vary with porosity as $s_{ij} = s^0_{ij}(1-\phi)^{-m}$.

To derive Eqs. (9), no speculation about Poisson's ratio was necessary. From Eqs. (3), it can be seen that the Poisson's ratios depend on ratios between the individual compliances and because the compliances depend on porosity in the same form, the Poisson's ratios do not depend on porosity. This agrees with the assumption discussed above (see Sec. II A).

Alternatively, from Eqs. (3) and Keating's relation if it is proposed that the key starting point is the assumption that Poisson's ratio is independent of porosity then all three compliances (and thus stiffnesses) must have an identical dependence on porosity. From Eqs. (9) it can be seen that (ignoring anisotropy in MS) all LA velocities in all directions will have the same dependence on porosity, hence the same κ, if the stiffnesses have identical porosity dependence. Our measurements are consistent with this assertion.

As for transverse acoustic (TA) velocities, dispersion with porosity due to the effect of MS is slightly stronger than for LA velocities as shown by Varadan *et al.*[35] This will give a slightly bigger κ for the porosity dependence of v'_T than for v'_L. The assertion is consistent with the literature results,[6,8,12,14] where the obtained value of κ_T is always bigger than the value of κ_L.

B. Analysis of results from the literature

In previous work, the porosity dependence of the velocity for TA waves along with that for LA waves has been measured or deduced, for various sample parameters. Fan *et al.*[12] obtain close κ-values for LA ($\kappa_L = 1.083$) and TA waves ($\kappa_T = 1.086$). Da Fonseca *et al.*[6,8] obtained $\kappa_L = 1.095$ with $\kappa_T = 1.19$. This latter value for TA waves was deduced via the Rayleigh wave velocity v_R in an acoustic microscopy experiment assuming isotropic PSi. The authors used the Victorov's relation: $v_R \approx v_T\left(0.718 - v_T^2/v_1^2\right)/\left(0.750 - v_T^2/v_1^2\right)$,

assuming an isotropic shear wave velocity $v_T^2 = c_{44}/\rho$. For bulk Si this relation gives $v_{0R}^{iso} = 5.07$ km/s. However, for anisotropic cubic crystals, v_R in (100) plane has to be deduced from Victorov's relation using $v_{T_\parallel[110]}^2 = \frac{1}{2}(c_{11} - c_{12})/\rho$ (see Ref. 34). For bulk Si this gives the correct value $v_{0R} = 4.15$ km/s – a result 20% lower than that obtained with the isotropic approach. As discussed above, PSi is anisotropic with $c_{44} > \frac{1}{2}(c_{11} - c_{12})$, thus, the value of c_{44} (and $v_{T[100]}$) deduced from v_R measured in (100) plane of PSi assuming it to be isotropic will be smaller (κ_T bigger) than the correct value.

For anisotropic cubic solids, the ratio $\eta = 2c_{44}/(c_{11} - c_{12})$ is the commonly defined anisotropy factor. It is equal to 1.56 for bulk Si (using values from the Table I), while for an isotropic solid $\eta = 1$. Our results above give a constant anisotropy for PSi with porosity (Eq. (15)). For (111)-oriented 2.7 μm thick sample with $\phi = 0.30$, Andrews *et al.*[10] found $\eta = 1.5$, which is close to the value for bulk Si.

Assuming anisotropy, Polomska[14] obtained for PSi $\kappa_L = 0.73 \pm 0.07$ with $\kappa_T = 0.9 \pm 0.1$. These values of κ for LA and TA waves overlap within the experimental error but with the measured value of κ_L smaller than κ_T. However, as Polomska used samples of small thickness (few micrometers) for Brillouin scattering measurements, there is a possibility that, in addition to the MS effect, negative velocity dispersion with thickness reported by Fan *et al.*[12] could affect the results. This experimentally observed dispersion was attributed to the presence of a transition layer between PSi film and Si substrate and is stronger for LA waves than for TA waves,[12] i.e., difference between κ_L and κ_T increases with decreasing thickness of PSi film below 10μm range.

The difference in LA and TA velocity dispersion with thickness and with porosity will affect the values of the anisotropy factor measured via acoustic waves. Compared with the "static" value, the reduction factor affecting c_{11} obtained from acoustic measurements is smaller than the factor reducing c_{44}. Thus, "acoustic" η will be smaller than the "static" one. This assertion is consistent with the literature results discussed above.

C. Dependence of the parameter κ on wafer resistivity

For the form of velocity dependence on porosity that we use, Phani *et al.*[36] noted that for composite materials κ depends on the microstructure of the porous material and its value for relatively well ordered structure lies between 0.5 and 1.5, with higher values corresponding to a more disordered structure. Thus we conclude that the values of κ that we obtained from velocity measurements are consistent with this overall understanding of the micro-morphology of PSi and the relationship that we present (Eq. (14)) allows the velocity, or level of disorder of the pore structure, to be predicted. This is especially useful when preparing PSi layers, for use as acoustic devices, from wafers of known resistivity.

For acoustic devices, e.g., a PSi Bragg reflector and a rugate filter[18,19] the characteristic impedance of an acoustic layer, $Z = \rho v'$, depends on mass density of the layer and the acoustic velocity in the layer, which depends on the porosity and morphology of the layer as shown above. Thus, a general dependence of κ on wafer resistivity is necessary if acoustic devices are to be successfully designed and etched. Using Eq. (12) the characteristic impedance can be expressed as $Z = Z_0(1 - \phi)^{\kappa+1}$.

In contrast, for passive optical devices, e.g., multilayers for optical filtering or sensing applications,[5,33] knowledge of the refractive index calculated from the porosity (or vice versa) is normally sufficient to characterize a sample or its constituent layers. This is the case because the effective medium methods for dielectric constant depend predominantly on the porosity of a layer with only a weak dependence on the micromorphology of the PSi.

D. Dependence of the parameter κ on HF concentration

It is known that the physical properties of electrochemically etched PSi depend on the concentration of HF in the etchant.[37] Thus, for a wafer of a given resistivity, the morphology—and hence κ -parameter controlling the acoustic impedance as a function of porosity—depends on the conditions of the wafer etching. For the wafer used with resistivity 15–25 mΩ cm it was possible for κ to increase or decrease showing the associated change in morphology versus HF concentration. We cannot explain the non-monotonic variation of κ with HF concentration for values just below 1. However, for future work it is clearly desirable to work in a region where there is not a strong dependence of κ on HF concentration so that it is not a critical parameter of the etching process.

V. CONCLUSIONS

This systematic experimental study of the porosity dependence of the elastic constants of PSi, with the accompanying theoretical considerations has shown that there is one form of porosity dependence obeyed by all the elastic constants in PSi as given in Eq. (15). Hence, the same porosity dependence applies for the anisotropic elastic moduli.

This is demonstrated by the fact that samples grown on wafers of different orientation, but with the same doping level, demonstrate the same dependence of LA velocity on porosity.

The fitting parameter κ, which is the exponent in the velocity dependence on porosity, depends on the doping level of the wafer from which the porous layer is etched and is also an indicator of the morphology of the PSi layer. We find that samples grown on wafers with different doping level have different morphology. The parameter κ depends on wafer resistivity as given in Eq. (14).

The parameter κ and thus morphology depends on the etching conditions via the HF concentration in the etchant.

The initial assumption that Poisson's ratio is effectively constant for PSi as porosity changes is validated by the constancy of the velocity-porosity dependence observed in the measured samples in different crystallographic directions. Additionally, we have shown that for PSi, considered as a cubic anisotropic material, all three elastic constants can be obtained by LA velocity measurements in any two principal directions by use of Keating's relation.

We have shown that velocity dispersion due to MS effect from pores must be considered as part of acoustic measurements of the elastic properties of PSi. We have estimated the order of magnitude of the effect by adapting existing theory on MS to the case of PSi.

Overall, the pleasing simplicity of the universal scaling of elastic constant with porosity clarifies the elastic properties of porous silicon. The results presented are consistent and explain variations in experimental results of previous studies on acoustic velocity in PSi. As a consequence of this work, acoustic devices depending on the velocity of sound in PSi can be designed for a wide range of Si wafer resistivity.

ACKNOWLEDGMENTS

We thank Professor J. J. Davies for useful comments.

[1]L. J. Gibson and M. F. Ashby, *Cellular Solids: Structure and Properties* (Cambridge University Press, Cambridge, 1999).
[2]D. Bellet, P. Lamagnère, A. Vincent, and Y. Bréchet, J. Appl. Phys. **80**, 3772 (1996).
[3]A. G. Cullis and L. T. Canham, Nature **353**, 335 (1991).
[4]T. H. Metzger, M. Binder, and J. Peisl, in *Properties of Porous Silicon*, edited by L. Canham (INSPEC, London, 1997), Chap. 3, p. 112.
[5]V. Torres-Costa and R. J. Martín-Palma, J. Mater. Sci. **45**, 2823 (2010).
[6]R. J. M. DaFonseca, J. M. Saurel, G. Deapaux, A. Foucaran, E. Massone, T. Taliercio, and P. Lefebvre, Superlattices Microstruct. **16**, 21 (1994).
[7]Y. Boumaiza, Z. Hadjoub, A. Doghmane, and L. Deboub, J. Mater. Sci. Lett. **18**, 295 (1999).
[8]R. J. M. DaFonseca, J. M. Saurel, A. Foucaran, J. Camassel, E. Massone, T. Taliercio, and Y. Boumaiza, J. Mater. Sci. **30**, 35 (1995).
[9]G. N. Aliev, B. Goller, D. Kovalev, and P. A. Snow, Phys. Status Solidi C **6**, 1670 (2009).
[10]G. T. Andrews, J. Zuk, H. Kiefte, M. J. Clouter, and E. Nossarzewska-Orlowska, Appl. Phys. Lett. **69**, 1217 (1996).
[11]D. J. Lockwood, M. H. Kuok, S. C. Ng, and Z. L. Rang, Phys. Rev. B **60**, 8878 (1999).
[12]H. J. Fan, M. H. Kuok, S. C. Ng, R. Boukherroub, J. M. Baribeau, J. W. Fraser, and D. J. Lockwood, Phys. Rev. B **65**, 165330 (2002).
[13]G. T. Andrews, A. M. Polomska, E. Vazsonyi, and J. Volk, Phys. Status Soidi A **204**, 1372 (2007).
[14]A. M. Polomska, "Elastic properties of porous silicon superlattices," Ph.D. thesis (Memorial University of Newfoundland, St. Johns, Newfoundland, 2010).
[15]K. Barla, R. Herino, G. Bomchil, J. C. Pfister, and A. Freund, J. Cryst. Growth **68**, 727 (1984).
[16]H. Cho, H. Sato, H. Nishino, Y. Tsukahara, M. Inaba, A. Sato, M. Takemoto, S. Nakano, and K. Yamanaka, IEEE Ultrasonic Symp. **1**, 757 (1995).
[17]C. Pramanik, T. Islam, H. Saha, J. Bhattacharya, S. Banerjee, and S. Dey, Proc. 18th Intern. Conf. on VLSI Design **3-7** (IEEE Computer Society, Kolkata, 2005), p. 235.
[18]G. N. Aliev, B. Goller, D. Kovalev, and P. A., Snow, Appl. Phys. Lett. **96**, 124101 (2010).
[19]L. Thomas, G. N. Aliev, and P. A. Snow, Appl. Phys. Lett. **97**, 173503 (2010).
[20]A. P. Roberts and E. J. Garboczi, J. Mech. Phys. Solids **50**, 33 (2002).
[21]M. L. Dunn and H. Ledbetter, Mater. Res. **10**, 2715 (1995).
[22]C. T. Herakovich and S. C. Baxter, J. Mater. Sci. **34**, 1595 (1999).
[23]J. F. Nye, *Physical Properties of Crystals* (Clarendon, Oxford, 1985).
[24]M. A. Hopcroft, W. D. Nix, and T. W. Kenny, Microelectromech. Syst. **19**, 229 (2010).
[25]A. Ballato, IEEE Trans. Ultrason. Ferroelect. Freq. Control **43**, 56 (1995).
[26]B. A. Auld, A*coustic Fields and Waves in Solids*, 2nd ed. (Krieger, Malabar, 1990), Vol. 1.
[27]P. N. Keating, Phys. Rev. **145**, 637 (1966).
[28]R. Truell, C. Elbaum, and B. B. Chick, *Ultrasonic Methods in Solid State Physics* (Academic, New York, 1969).
[29]C. M. Sayers, J. Phys. D: Appl. Phys. **14**, 413 (1981).
[30]P. C. Waterman and R. Truell, J. Math. Phys. **2**, 512 (1961).
[31]D. A. G. Bruggeman, Ann. Phys. **24**, 636 (1935).
[32]S. D. Lambade, G. G. Sahasrabudhe, and S. Rajagopalan, Phys. Rev. B **51**, 15861 (1995).
[33]V. Lehmann, *Electrochemistry of Silicon* (Wiley -VCH, Weinheim, 2002).
[34]L Gold, Phys. Rev. **104**, 1532 (1956).
[35]V. K. Varadan, Y. Ma, and V. V. Varadan, Pageoph **131**, 577 (1989).
[36]K. K. Phani, S. K. Niyogi, A. K. Maitra, and M. Roychaudhury, J. Mater. Sci. **21**, 4335 (1986).
[37]H. Aoyagi, A. Motohashi, A. Kinoshita, T. Aono, and A. Satou, Jpn. J. Appl. Phys. **32**, L1 (1993).